Superalloys 2008
Roger C. Reed, Kenneth A. Green, Pierre Caron, Timothy P. Gabb, Michael G. Fahrmann, Eric S. Huron and Shiela A. Woodard
TMS (The Minerals, Metals & Materials Society), 2008

A Modeling Tool for the Precipitation Simulations of Superalloys during Heat Treatments

Kaisheng Wu[1], Fan Zhang[1], Shuanglin Chen[1], Weisheng Cao[1] and Y. A. Chang[2]

[1]CompuTherm LLC, 437 S. Yellowstone Dr., Ste 217, Madison, WI 53719
[2]Department of Materials Science and Engineering, University of Wisconsin-Madison, 1509 University Ave., Madison, WI 53706

Keywords: computer modeling, precipitation modeling, heat treatment, Alloy 718

Abstract

The understanding and control of the precipitation of secondary phases during heat treatments is critical for the properties of age-hardening superalloys. A modeling tool has been developed to simulate the complicated precipitations and microstructure evolutions during arbitrary thermal histories. It integrates both thermodynamic and kinetic calculations with available multi-component and multiphase databases. Its major simulation functionalities have been demonstrated by calculating the precipitation kinetics in Alloy 718. The advantages and limitations are also discussed.

Introduction

Precipitation hardening is one of the most important strengthening mechanisms for the Ni-based superalloys. Its success relies on the formation and distribution of the strengthening phases, such as $L1_2$ γ′ and DO_{22} γ″ phases, which are mostly coherent or semi-coherent with the f.c.c. matrix phase. An optimum size and amount of these strengthening phases are obtained by a deliberately designed heat treatment scheme. A thorough understanding and careful control of the precipitation microstructures during heat treatments is thus critical for the properties of age-hardening superalloys.

Helpful as it is to understand the microstructure, the knowledge of thermodynamic and kinetic theories can be extremely difficult for engineers to apply to commercial superalloys which, to achieve a wide variety of property requirements, usually consist of more than 10 alloy elements. These multi-component and multiphase systems make the microstructures complicated. In most cases, therefore, experimental trial and error seems inevitable, but the soaring cost of the raw materials and equipment setup makes the expense skyrocketed. Computational tools, developed by combining reliable experimental evidence with reasonable theoretical basis, are thus becoming an increasingly important substitute for the experiment at a small fraction of cost.

In the current paper we present a modeling tool that has been developed to simulate the complicated precipitations and microstructure evolutions during arbitrary thermal histories. The modeling tool, which is part of the Pandat™ software[1], integrates both thermodynamic and kinetic calculations. One unique feature of this modeling tool that offers tremendous help for alloy design is a global optimization module for search of the best or worst scenario given alloy chemistry range and heat treatment conditions. The package is designed for generalized applications while in this paper the investigation is focused on Alloy 718.

The Models

Thermodynamic Models and Database Development

Thermodynamic calculation is based on Calphad approach[2, 3]. The theoretical basis of thermodynamic calculations rests on the fact that the location of a phase boundary is the result of stability competition between two or more phases.

A thermodynamic database, which stores the Gibbs energy of each individual phase in the alloy system, is developed using a phenomenological approach. Its establishment starts with deriving thermodynamic models for all the constituent binary systems. A model type is selected to correspond with the physical and thermodynamic properties of a specific phase. Two of the most common phase types in metallic alloys are disordered solid solutions (e.g., γ phase in Ni-base superalloys) and ordered intermetallic phases (e.g., γ′, γ″ and δ).

A disordered solution phase is described by a substitutional type model [4]. The Gibbs energy of such a phase in a binary system can be written as:

$$G_m^{\phi} = \sum_{i=A,B} x_i G_i^{\phi,0} + RT \sum_{i=A,B} x_i ln x_i + \sum_v L_v (x_A - x_B)^v \quad (1)$$

where the first term on the right hand side of the equation represents the reference state with x_i the mole fraction of component i, and $G_i^{\phi,0}$ the Gibbs energy of pure component i with ϕ structure; the second term is the ideal mixing term with R the gas constant, and T the temperature; the last term is the excess Gibbs energy of mixing with L_v the interaction coefficient, and v the power of the polynomial series. When $v = 0$, it is a regular solution model, and when $v = 0$ and 1, it is a sub-regular solution model, and so on. The model parameters are optimized to give the best fit to the available experimental data.

An ordered intermetallic phase is described by a variety of sublattice models, such as the compound energy model [4, 5] and the bond energy model [6, 7]. In these models the Gibbs energy is a function of the sublattice species concentrations and temperature. The Gibbs energy of a binary intermetallic phase described by a two-sublattice compound energy model, $(A, B)_p : (A, B)q$, can be written as:

$$
\begin{aligned}
G_m^{\phi} = & \sum_{i=A,B} \sum_{j=A,B} y_i^I y_j^{II} G_{i:j}^{\phi} \\
& + RT \left[\frac{p}{p+q} \sum_{i=A,B} y_i^I \ln y_i^I + \frac{q}{p+q} \sum_{i=A,B} y_i^{II} \ln y_i^{II} \right] \\
& + \sum_{j=A,B} y_A^I y_B^I y_j^{II} \left(y_A^I - y_B^I \right)^v L_{A,B:j}^v \\
& + \sum_{i=A,B} y_i^I y_A^{II} y_B^{II} \left(y_A^{II} - y_B^{II} \right)^v L_{i:A,B}^v \\
& + y_A^I y_B^I y_A^{II} y_B^{II} L_{A,B:A,B}
\end{aligned} \tag{2}
$$

where y_i^I and y_i^{II} are the species concentrations of component i in the first and second sublattices, respectively. The first term on the right hand side of the equation represents the reference state with the mechanical mixture of the pure compounds: A, A_pB_q, B_pA_q, and B. $G_{i:j}^{\phi}$ is the Gibbs energy of the stoichiometric compound i_pj_q with ϕ structure. The value of $G_{i:j}^{\phi}$ can be obtained experimentally if i_pj_q is a stable compound, or it can be a model parameter obtained by optimization using experimental data related to this phase. Recently, *'ab initio'* calculations have also been used to obtain such a value for an unstable i_pj_q compound.

After thermodynamic descriptions for all the constituent binaries are established, preliminary descriptions for the ternaries are obtained by the extrapolation of the binary model parameters using geometric models, such as the Muggianu model[8]. Ternary interaction model parameters are introduced to better describe the ternary system when reliable experimental data are available. The same strategy applies to the high-order systems.

Multi-component thermodynamic database for nickel alloys has been developed and applied to Alloy 718 in this wok. The mobility database for the nickel alloy systems is based on the database developed by Campbell et al.[9] at NIST. This database was modified slightly to be consistent with the thermodynamic database developed at CompuTherm. In addition, it is also validated and improved using the recently published mobility data by Reed and his colleagues [10, 11]. In the example shown in Figure 1, the interdiffusion coefficient of Ni-Pt alloys are calculated by our current database and compared with the experimental data[10]. Excellent agreement is obtained for temperatures above 1000°C.

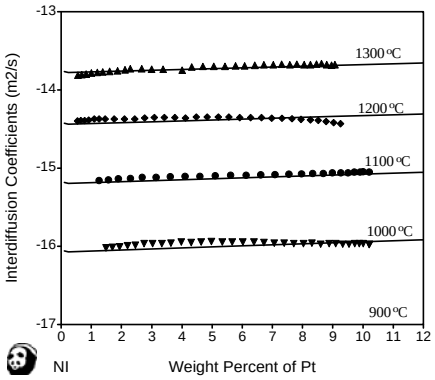

Figure 1 Comparison of calculated interdiffusion coefficient in Ni-Pt system with experimental data[10]

Kinetic Simulations

Models

The kinetic simulation employs three models to treat three concomitant events: nucleation, growth/dissolution and coarsening. For Alloy 718, three primary precipitate phases, γ″, γ′, and δ, have been modeled simultaneously. Moreover, two types of δ have been treated, one nucleating at grain boundaries and one transformed from metastable γ″.

The nucleation is described on the basis of the classical nucleation theory, which gives the transient nucleation rate as

$$
J = Z\beta^* N_c \exp\left(-\frac{\Delta G^*}{kT}\right) \exp\left(-\frac{\tau}{t}\right) \tag{3}
$$

where Z is the Zeldovich factor, β^* is the atomic attachment rate, N_c is the nucleation site density, ΔG^* is the critical nucleation barrier, k is the Boltzmann constant, T is the absolute temperature, t is the time and τ is the incubation time.

The multi-component version of some of the parameters in Eq. (3), including the incubation time, has been proposed by Kozeschnik et al[12]. Their formulations are employed in the current model. The nucleation site density and nucleation driving force are modified to deal with nucleation at grain boundaries(e.g., grain boundary δ) and transformation from metastable phase(e.g., transformed δ).

The multi-component growth model is modified based on that proposed by Morral and Purdy[13], so that it is able to treat the growth/dissolution of various precipitate phases with different morphologies. For example, the γ′ phase is treated as sphere, γ″ and grain boundary δ as lens with constant aspect ratio, and transformed δ as plate with variable aspect ratio.

The motion rate of the curved interface, e.g., the interface of a spherical or lens-like precipitate, and the edge of a plate-like precipitate, is described by

$$
v = \frac{K}{R}\left(\frac{1}{R^*} - \frac{1}{R}\right) \tag{4}
$$

with

$$
K = \frac{2\sigma V_m^{\alpha}}{\left(\Delta C^{\alpha\beta}\right]\left[M\right]^{-1}\left[\Delta C^{\alpha\beta}\right)} \tag{5}
$$

where R is the average radius of the interface, R^* is the size of the critical nuclei, σ is the interfacial energy between the matrix phase α and precipitate phase β, V_m^{α} is the molar volume of the matrix phase α. $\left(\Delta C^{\alpha\beta}\right]$ and $\left[\Delta C^{\alpha\beta}\right)$ are row and column vector of the solute concentration difference between the precipitate phase β and the matrix phase α, and $[M]$ is the chemical mobility matrix.

The motion rate of a planar interface, e.g., thickening of the plate, is described by

$$v = \frac{K'}{h} \tag{6}$$

with

$$K' = \frac{\Delta G_m^*}{\left(\Delta C^{\alpha\beta}\right)\left[M\right]^{-1}\left[\Delta C^{\alpha\beta}\right)} \tag{7}$$

where h is the half thickness of the plate, and ΔG_m^* is the transformation driving force.

The coarsening model characterizes the curvature-driven particle growth, and is based on the LSW theory[14, 15]. The multi-component version can be written as

$$R^3 - R_0^3 = \frac{2}{9}Kt \tag{8}$$

where R is the average radius of the spherical particles, R_0 is the "initial" size when the system is close to the equilibrium, t is time, and K is the kinetic parameter defined in Eq.(5).

Mass Conservation

At each time step, there are fraction changes of the precipitate phases and hence super-saturation changes of the matrix phase. These can be easily updated by mass conservation equation:

$$C_i^0 = \left(1 - \sum_j^{n_p} \phi_j\right) C_i^\alpha + \sum_j^{n_p} \phi_j C_i^j \tag{9}$$

where C_i^0 is the initial alloy composition (mole fraction) of component i, ϕ_j is the mole fraction of precipitate phase j, n_p is the number of precipitate phases, C_i^α is the mole fraction of component i in the matrix phase α, and C_i^j is the mole fraction of component i in precipitate phase j.

Numerical Calculations

The simulation is carried out by solving Eqs.(3), (4), (6), (8) and (9) simultaneously at each time step. A modified Runge-Kutta 5th-order algorithm[16] is employed to adjust the time step to assure the accuracy and efficiency. As a result, at the early stage where nucleation and growth are dominant, a small time step is used to catch the dramatic fraction changes of the precipitate phases, while at a late stage where coarsening prevails, a time step likely several orders of magnitude larger is sufficient for an accurate calculation. The thermodynamic calculation is fully integrated to update the necessary parameters including nucleation driving force, supersaturation of the matrix phase, and solute partitioning among the matrix and precipitate phases. The mobility changes of the alloy elements due to the saturation changes of the matrix phase are updated as well through the available kinetic database.

Global Search Model

Another unique functionality that the software offers is a Global Search Module. It efficiently combines a deterministic optimization algorithm[17, 18] with thermodynamic and kinetic calculations. It automatically searches the extreme values of size/fraction of precipitate phases within a multi-dimensional composition and time range under given heat treatments, hence offering valuable guidance for designing alloy chemistry and processing conditions.

Results for Alloy 718

Thermodynamic Calculations

Tables I-III show the comparison between the calculated and experimentally determined equilibrium composition for γ, γ′, and γ′′. The calculation of the metastable γ′′ phase is carried out by suspending the corresponding stable δ phase.

The calculated contents for most elements agree reasonably well with those determined by atom probe measurements[19], especially at higher temperature (718°C). The low temperature results (621°C) show some deviations, which are more evident for some refractory elements such as Mo. As discussed by Miller and Babu[19], due to the multistep heat treatment and relatively short heat treatment time, it is not unlikely that equilibrium might not be reached during the measurement, which leads to the difference between calculated and measured phase composition. Furthermore, Cr and Mo enriched σ phase was predicted to be stable by the calculation, while it was not identified in the experiment of [19]. This is due to the sluggish kinetics of σ phase. In order to compare with the experimental data of [19], σ phase was suspended in this calculation.

As discussed elsewhere, δ phase is thermodynamically stable, and γ″ will transform to δ due to long time exposure at high temperature. To better understand the transformation between them, thermodynamic descriptions for both of these two phases are important. Figure 2 shows the fraction of δ phase as a function of temperature for one 718 alloy. The experimental data[20] are also plotted for comparison. Clearly an excellent agreement has been obtained.

Table I: Phase chemistry of the γ phase

718 °C (at%)							
	Al	Co	Cr	Fe	Mo	Nb	Ti
Cal	0.43	0.38	23.5	26.5	2.12	0.96	0.13
Exp[19]	0.58±0.03	0.38±0.02	23.48±0.17	25.54±0.18	2.13±0.05	1.59±0.04	0.47±0.02
621 °C (at%)							
	Al	Co	Cr	Fe	Mo	Nb	Ti
Cal	0.23	0.39	23.1	27.9	2.2	0.46	0.04
Exp[19]	0.34±0.02	0.47±0.02	25.25±0.17	26.92±0.17	2.5±0.05	0.99±0.03	0.21±0.01

Table II: Phase chemistry of the γ′ phase

718 °C (at%)							
	Al	Co	Cr	Fe	Mo	Nb	Ti
Cal	8.09	0.08	0.91	1.91	0.1	7.4	7.74
Exp[19]	9.11±0.27	0.09±0.03	0.79±0.08	2.0±0.13	0.53±0.07	7.22±0.24	7.38±0.25
621 °C (at%)							
	Al	Co	Cr	Fe	Mo	Nb	Ti
Cal	8.3	0.06	0.91	1.96	0.1	6.7	7.8
Exp[19]	8.79±0.46	0.1±0.05	0.83±0.14	2.24±0.23	1.38±0.18	7.54±0.43	8.24±0.44

Table III: Phase chemistry of the γ″ phase

718 °C (at%)							
	Al	Co	Cr	Fe	Mo	Nb	Ti
Cal	0.41	0.04	0.85	1.13	0.5	18.9	4.16
Exp[19]	0.35±0.09	0.05±0.03	2.16±0.22	2.11±0.22	1.3±0.17	20.07±0.68	5.59±0.36
621 °C (at%)							
	Al	Co	Cr	Fe	Mo	Nb	Ti
Cal	0.22	0.09	1.1	1.29	0.34	20.0	2.93
Exp[19]	0.44±0.1	0.19±0.07	1.93±0.22	1.73±0.2	3.0±0.27	19.27±0.68	4.73±0.34

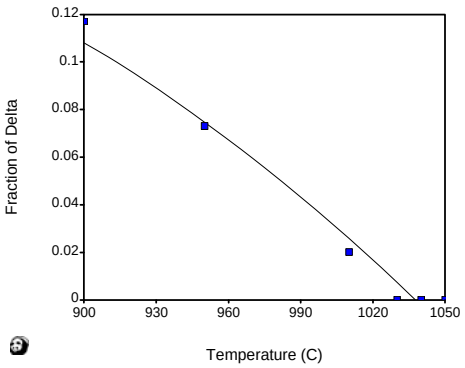

Figure 2 Fraction of δ phase as a function of temperature. Experimental data are from M. Stockinger et al, in Superalloys 718, 625, 706 and Various Derivatives Edited by E. A. Loria, TMS 2001, p 141-148

Kinetic Calculations

Seven components, Ni-Fe-Cr-Al-Nb-Mo-Ti, have been chosen to carry out the kinetic calculations. Three major precipitate phases, γ′, γ″ and δ, are considered. According to the experimental information[21-23], γ′ particles are treated as spherical shape, and γ″ particles are treated as lens-like shape with a constant aspect ratio (thickness/length ratio) of 1/9~1/10. Both phases are considered to nucleate homogeneously within the matrix phase. Two types of δ phase are treated simultaneously. One is for those forming at the grain boundary, which is treated as lens-shape with constant aspect ratio. The other is for those transforming from the metastable γ″, which is treated as plate with time-varying aspect ratio.

The calculated temporal evolutions of the average size for γ″ and γ′ have been compared with experimental data[23] in Figure 3. The size of γ″ is characterized by the particle length, while that of γ′ sphere is characterized by its diameter. The heat treatment is isothermal annealing at three different temperatures, 700°C, 725°C and 750°C, respectively.

Results for both phases show an excellent agreement at the medium temperature (725°C). The calculated size change of γ′ phase is obviously in a better fit than that of γ″, as shown in Figure 3. The reason is partly due to the varying aspect ratios of the γ″ lenses which are observed to be dependent on alloy composition[22]. Most likely they are also dependent on temperature and annealing time considering the change of the coherency between the γ″ particle and γ matrix. The approximation of constant aspect ratio may therefore cause some artifacts. Despite the discrepancies, however, the overall agreement is still satisfactory.

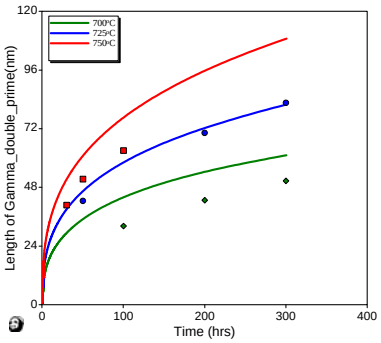

(a)

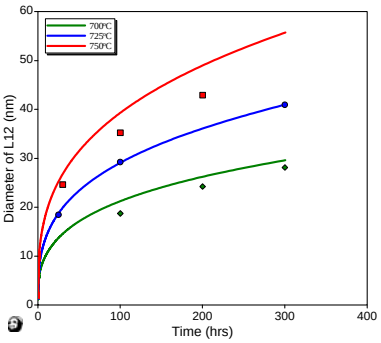

(b)

Figure 3 Average size changes of (a)γ″ and (b)γ′ phases under temperatures 700°C(green line for calculated, green solid diamonds for experimental data), 725°C(blue line for calculated, blue solid spheres for experimental data), and 750°C(red line for calculated, red solid squares for experimental data). The experimental data are taken from Han et al., Metal Science, 16, 555(1982)

The T-T-T diagram for Alloy 718 can also be calculated, as shown in Figure 4. The alloy composition is chosen from that given by Han et al.[23]. Only the starting curves, with a criterion of 1% of volume fraction of the corresponding phases, are plotted in Figure 4, though the finish curves can also be calculated easily.

The comparison of the calculated results with the experimental determination[24] is shown in Figure 5. Two curves pointed by arrows in Figure 5a and Figure 5b are starting curves for γ′+γ″ and γ′+γ″+δ regions, respectively. A good agreement is obtained considering the nose positions, which are the most confident experimental values.

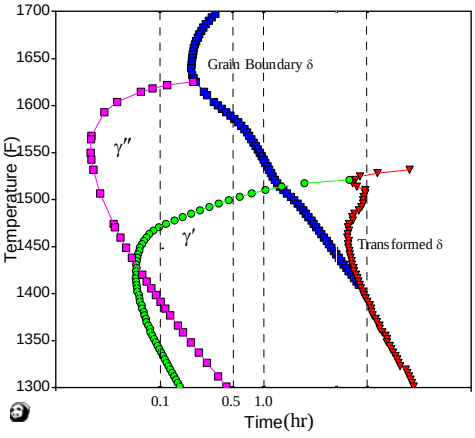

Figure 4 Calculated T-T-T Diagram for Alloy 718.

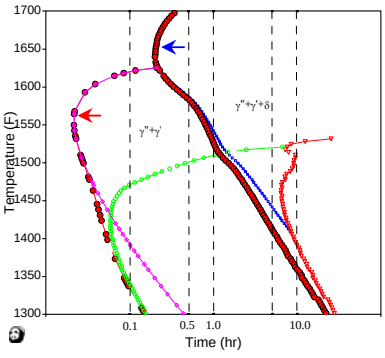

(a)

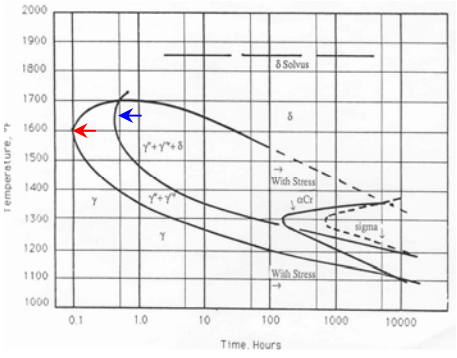

(b)

Figure 5 Comparison of (a) the Calculated T-T-T Diagram for Alloy 718 and (b) the experimental one from A. Oradei-Basile, and J. F. Radavich, in Superalloys 718, 625 and Various Derivatives, edited by E. A. Loria (The TMS Society, 1991), pp. 325.

The global search module has been used to search the range of precipitate sizes within a given composition range. The composition range is chosen according to the sample compositions in the experiments[22]. The results are compared with experimental data[22] in Figure 6. The black line is the low bound of the average size change with time, while the blue dashed line is that of the high bound. The heat treatment is isothermal annealing at 760^{o}C. A series of alloys with different chemistries within the above listed composition range were annealed for 100hrs, and the average sizes were measured as plotted on the figures. The predicted size range for the γ′ precipitates agree with the experimental measurements fairly well, except for one data point with a value far lower than others(Figure 6(b)). The measured γ″ sizes (Figure 6(a)) are more scattered, partly due to the difficulties in measurements for lens shape particles. The calculated results give a more conservative prediction in view of the possible experimental uncertainties.

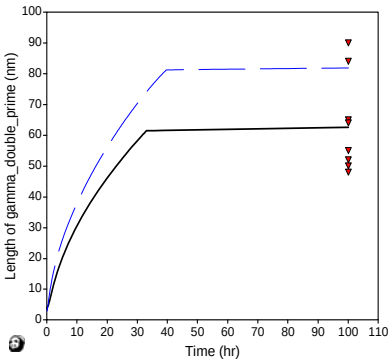

(a)

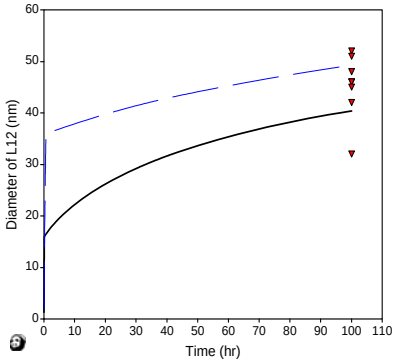

(b)

Figure 6 Comparison of the calculated size range of (a) γ″ and (b) γ′. The experimental data are from Collier et al., *Superalloy 1988*, pp43-52.

Discussion

The calculated results reveal the capabilities of the current software package for integrated thermodynamic and kinetic simulations. These capabilities offer reliable information for engineers to fine tune alloy chemistry and processing schedules at a well affordable cost. It handles the co-precipitation of phases with various morphologies by fully considering their mutual interactions. These interrelated effects are reflected by the parameters including, but not restricted to, nucleation site density and nucleation activation energy (Nc and ΔG^* in Eq. (3)), growth mobility and solute partitioning ($[M]$ and $\left(\Delta C^{\alpha\beta}\right]$ in Eq. (5)), etc. It is thus more flexible and extensible than the simplified analytic solutions or linear regression model. In addition, thermodynamic driving forces for all the precipitates are accurately calculated with varying compositions and temperatures due to the direct integration of thermodynamic calculation and kinetic simulation. Although most of calculated results in the previous section are under isothermal conditions, the heat treatment options are arbitrary including complicated multi-stage non-isothermal histories. The global search functionality is also extremely helpful to seek the best and worst scenario within a composition range.

Nevertheless, cautions should have to be taken, just as for any software products. First of all, reliable thermodynamic and kinetic databases are prerequisite for the success of the precipitation simulation. These databases are available that cover almost all of the important alloying elements and phases, but not without limitations. The CALPHAD approach to building a database for multi-component systems involves modeling of a huge amount of binary, ternary, and higher-order systems. To model all the systems is impossible in a person's life span. Meanwhile, the accuracy of the database relies on the model parameters that correctly describe the existing experimental data. As a result, a reasonable way is to focus on some key systems that are important for industrial applications and have abundant experimental information. Application to composition ranges that are outside what these key systems cover, therefore, can be risky.

Secondly, a number of critical parameters are, inevitably as all the modeling tools, adjusted for a better fit to the experimental results. These parameters include interfacial energy, molar volume, and nucleation site density of precipitate phases. These adjusted values are included in the property databases that are still under development. Again, to establish these databases require exhaustive validation against some clearly defined precipitation experiment data. Unfortunately the authors found that it is hard to find those experimental data. An alternative strategy of the current software is to provide a user interface so that users can input these properties interactively. The values can be chosen in such a way that the calculated coarsening behavior matches the experimental results.

As scarce experimental information in the public domain is available for calibration purpose, it is not unusual that users find their own proprietary models to be more reliable for a specific alloy system. To serve this demand, the software provides a way for users to input their own kinetic models via a specifically designed script file. This added flexibility greatly facilitates users to incorporate their proprietary models with the software for prerequisite thermodynamic and kinetic inputs.

The models used in the current paper calculate the temporal evolution of the average size of the precipitate phases. In many cases, especially in Ni-base superalloys, the size distribution of the precipitate phases, most importantly that of γ′ phase, is directly tailored to control the final mechanical properties. A model on the basis of the work by Kampmann and Wagner[25] is also developed to meet this need. Since no reliable experimental information on the size distribution of precipitate phases in Alloy 718 has been found to be compared with, the calculations using this model is not included in the current paper.

Summary

An advanced and user-friendly software package has been developed for precipitation heat treatment simulations. It offers a variety of functionalities that facilitate engineers to design alloy chemistry and heat treatments to meet the property demands. Its advantages include

1. Thermodynamic and kinetic databases that cover almost all of key alloy elements and phases in Ni-base superalloys have been developed.

2. An improved accuracy is achieved by on-time update of nucleation driving forces, transformation driving forces, mobilities and other properties.

3. The models are designed for multi-component and multiphase cases, with detailed considerations of their interactions.

4. An interface is provided for users' own proprietary models.

5. A global search module enables users to search the best and worst scenario within a given composition range and heat treatment schedule.

It can not be over emphasized, nevertheless, the importance of well designed experiments for validations and calibrations of the kinetic models. Lack of some key properties such as interfacial energies is also a concern and has been considered for the ongoing development effort.

Acknowledgement

The authors would like to acknowledge the financial support of AFRL through SBIR contract: FA8650-05-C-5202. We would like to thank Drs. J. Simmons, P.Martin, and D. Ballard of AFRL for their interest and guidance of this work, and Dr. D. Furrer and Prof. Radavich for their valuable suggestions and discussions.

References

1. S. L. Chen, S. Daniel, F. Zhang, et al., CALPHAD: Computer Coupling of Phase Diagrams and Thermochemistry **26**, 175 (2002).
2. L. Kaufman and H. Bernstein, *Computer Calculation of Phase Diagrams* (Academic Press, New York, 1970).
3. N. Saunders and A. P. Miodownik, *CALPHAD-Calculation of Phase Diagrams, A Comprehensive Guide* (Pergamon Press, New York, 1998).
4. I. Ansara, Int. Metals Rev. **24**, 20 (1979).
5. B. Sundman and P. Willemin, Acta Metall. **36**, 977 (1988).
6. W. A. Oates and H. Wenzl, CALPHAD **16**, 73 (1992).
7. S.-L. Chen, C. R. Kao, and Y. A. Chang, Intermetallics **3**, 233 (1995).
8. Y. M. Muggianu, M. Gambino, and L. P. Bros, J. Chim. Phus. **72**, 85 (1975).
9. C. E. Campbell, W. J. Boettinger, and U. R. Kattner, Acta Mater. **50**, 775 (2002).
10. M. S. A. Karunaratne and R. C. Reed, Acta Mater. **51**, 2905 (2003).
11. M. Krcmar, C. L. Fu, A. Janotti, et al., Acta Mater. **53**, 2369 (2005).
12. E. Kozeschnik, I. Holzer, and B. Sonderegger, J. Phase Equil. Diff. **28**, 64 (2007).
13. J. E. Morral and G. R. Purdy, Scripta Metall. Mater. **30**, 905 (1994).
14. I. M. Lifshitz and V. V. Slyozov, J. Phys. Chem. Solids **15**, 35 (1961).
15. C. Wagner, Z. Elektrochem. **65**, 581 (1961).
16. W. H. Press, S. A. Teukolsky, W. T. Vetterling, et al., in *Numerical Recipies in C: The Art of Scientific Computing* (Cambridge University Press, New York, 1992), p. 716.
17. R. Horst, P. M. Pardalos, and N. V. Thoai, *Introduction to Global Optimization* (Kluwer Academic Publishers, 1995).
18. R. Horst and H. Tuy, *Global Optimization: Deterministic Approaches* (Springer, 2003).
19. M. K. Miller and S. S. Babu, in *Superalloys 718, 625, 706 and Various Derivatives*, edited by E. A. Loria (TMS, 2001), p. 357.
20. M. Stockinger, E. Kozeschnik, B. Buchmayr, et al., in *Superalloys 718, 625, 706 and Various Derivatives*, edited by E. A. Loria (TMS, 2001), p. 141.
21. I. Kirman and D. H. Warrington, Metallurgical Transactions **1**, 2667 (1970).
22. J. P. Collier, A. O. Selius, and J. K. Tien, in *Superalloys 1988*, edited by S. Reichman, D. N. Duhl, G. Maurer, S. Antolovich and C. Lund (The Metallurgical Society, 1988), p. 43.
23. Y.-f. Han, P. Deb, and M. C. Chaturvedi, Metal Science **16**, 555 (1982).
24. A. Oradei-Basile and J. F. Radavich, in *Superalloys 718, 625 and Various Derivatives*, edited by E. A. Loria (The TMS Society, 1991), p. 325.
25. R. Kampmann and R. Wagner, in *Decomposition of alloys: the early stages*, edited by P. Haasen, V. Gerold, R. Wagner and M. F. Ashby (Pergamon Press, Oxford, 1984), p. 91.